Angular Momentum of Galaxies in the Densest Environments: A FLAMES/GIRAFFE IFS Study of the Massive Cluster Abell 1689 at z = 0.18

Francesco D'Eugenio[1]
Ryan C. W. Houghton[1]
Roger L. Davies[1]
Elena Dalla Bontà[2, 3]

[1] Sub-department of Astrophysics, Department of Physics, University of Oxford, United Kingdom
[2] Dipartimento di Fisica e Astronomia "G. Galilei", Università degli Studi di Padova, Italy
[3] INAF–Osservatorio Astronomico di Padova, Italy

Early-type galaxies (ETGs) exhibit kinematically distinct slow and fast rotator (SR, FR) morphologies. The former are much less common (10 % of ETGs), but their incidence is higher in the core of the Virgo Cluster (25 %). Here we present FLAMES/GIRAFFE integral field spectroscopy of 30 galaxies in the massive cluster Abell 1689 at z = 0.183. Abell 1689 has a density 30 times higher than that of Virgo, making it the ideal place to test the effects of environment, such as local density and cluster properties. We find 4.5 ± 1.0 SRs (or an average ETG fraction, f_{SR}, of 0.15 ± 0.03) in Abell 1689, identical to the value for field/groups in ATLAS^{3D}. Within Abell 1689 f_{SR} increases towards the centre, exceeding the value found in the core of Virgo. This work is the highest redshift study of its kind.

Kinematical classification of ETGs

ETGs comprise morphologically distinct elliptical (E) and lenticular (S0) galaxies. Despite their differences, Es and S0s have lots in common. They are both characterised by old stellar populations, which has earned them the attribute "early-type". The average ETG has little or no cold gas, which is reflected in the star formation rate. Its light profile is smooth and its shape fairly regular. One of the most puzzling facts about these galaxies is how, with masses and luminosities that span several orders of magnitude, they obey a number of tight scaling relations. These include the colour–magnitude relation, the colour–σ and Mg–σ relations (where σ is the velocity dispersion) and the fundamental plane. The mere existence of these empirical laws — alongside their very small scatter — imposes strong constraints on the structure and evolution of ETGs (Bower et al., 1992). This makes them ideal testing grounds for any galaxy formation theory. Their study, important in its own right, is also fundamental for our understanding of the process of structure formation in the Universe.

The advent of integral field spectroscopy (IFS) started a revolution in the study of ETGs. The SAURON survey discovered the existence of two kinematically distinct classes of ETGs, slow and fast rotators (SRs and FRs, see Emsellem et al. [2007]) and Cappellari et al. (2007). The former have little or no rotation, exhibit kinematically decoupled cores and misalignment between kinematics and photometry. The latter are flattened systems, compatible with rotational symmetry and a disc-type origin. The new division crucially crosses the boundary between Es and S0s, in that FRs populate both morphological classes. ATLAS^{3D} (the volume-limited follow-up survey to SAURON; Cappellari et al., 2011a; Emsellem et al., 2011), established that 66 % of morphological ellipticals are FRs, and thus share the same internal structure as S0s. This is evidence for a new classification paradigm, based on kinematics rather than morphology (Cappellari et al., 2011b).

The ATLAS^{3D} team presented the kinematic morphology–density (kT–Σ) relation, analogous to the morphology–density relation (Dressler, 1980). It links the fraction of SRs in the ETG population (f_{SR}) with the local number density of galaxies: they found that f_{SR} is independent of the environment density over five orders of magnitude from field to group environments. But they noticed a sharp increase in f_{SR} in the inner core of the Virgo Cluster, the highest density probed by the ATLAS^{3D} survey. Virgo is an unrelaxed, low-density cluster, but what would be measured in the denser environments beyond the local Universe? Addressing this question gives further insight on the kT–Σ relation, and on the processes that drive galaxy formation and evolution.

Since rich, relaxed clusters are rare, they can only be found at higher redshifts. The multiplexing capabilities of FLAMES/GIRAFFE (Pasquini et al., 2002), combined with the collecting power of the ESO Very Large Telescope (VLT), are the ideal tools for this task.

FLAMES/GIRAFFE observations of Abell 1689

Abell 1689, a massive galaxy cluster at redshift z = 0.183, has regular, concentric X-ray contours suggesting that it is relaxed. Its X-ray luminosity outshines Coma by a factor of three, and Virgo by over an order of magnitude. Its comoving distance is 740 Mpc, giving a scale of 1 arcsecond per 3.0 kpc. Alongside its physical properties, Abell 1689 was an ideal target for FLAMES because the spatial resolution of the GIRAFFE-deployable integral field units (IFUs) samples up to one effective radius (R_e) for most galaxies. Finally, a wealth of archival data, including imaging from the Hubble Space Telescope (HST) Advanced Camera for Surveys (ACS), is available and vital to a study of this nature.

F625W-band imaging from the HST ACS, combined with g'- and r'-band GEMINI imaging were used for the photometry (Houghton et al., 2012). The spectroscopic data (spectral resolution, R = 11 800, spectral range 573 nm < λ < 652 nm [486 nm < λ < 552 nm rest frame]) covers standard V-band absorption features. GIRAFFE provides 15 independent mini IFUs, deployable anywhere on the focal plane; each IFU is positioned by a magnetic button and contains an array of 20 square microlenses. They are arranged in four rows of six (with four "dead" corners) for a total field of view of 3 by 2 arcseconds. Each lenslet is then connected to the spectrometer with a dedicated optical fibre bundle. Alongside the 15 IFUs, the instrument also provides 15 fully deployable sky fibres.

Since the magnetic buttons are larger (10 arcseconds) than the IFU field of view, they cannot be deployed closer than a minimum distance of 11 arcseconds. GIRAFFE permits the observer to target 15 objects simultaneously and we chose to target 30 galaxies as a compromise between sample statistics and integration time. In order to gain the maximum possible signal-to-noise ratio, we initially selected the 30 ETGs with the highest

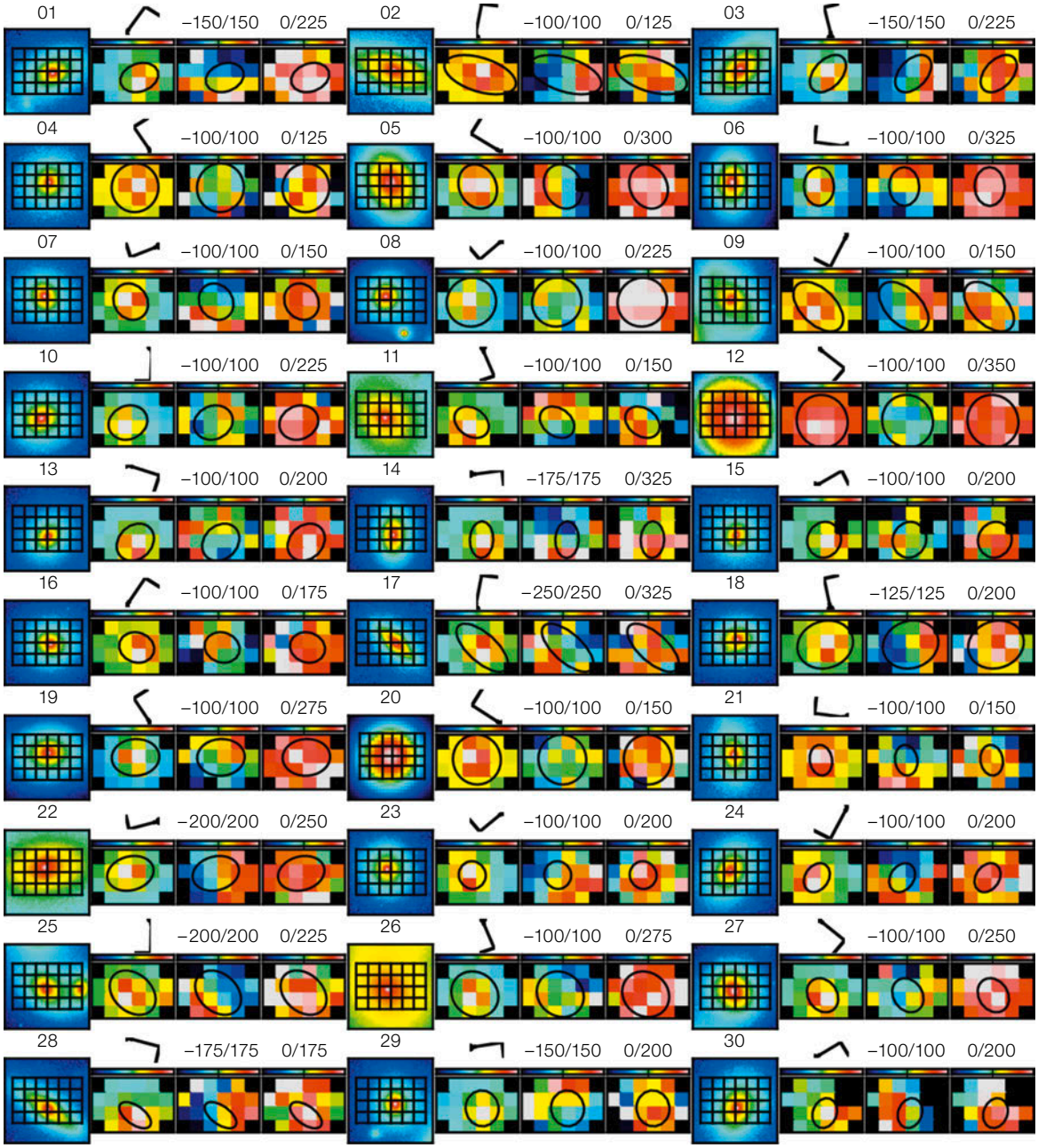

Figure 1. Kinematic maps of the Abell 1689 sample. For each of the 30 galaxies in the sample we present a set of four images. The first one shows FLAMES/GIRAFFE IFU footprints superimposed on HST imaging (Gemini imaging for target 20). The second plot shows the reconstructed image from VLT integral field spectroscopy, where each square is a spaxel and corresponds to a lenslet of the IFU. Also shown is an isophote at either R_e, or the closest integer fraction that fits into the IFU footprint. The four black corners correspond to unavailable "dead" spaxels, while other black spaxels (seen in 11, 15 and 30) correspond to broken or unused fibres. Velocity and velocity dispersion maps are depicted in the third and fourth plots. The black compass arrows show north and east directions. Colour-bar limits are given in km/s.

surface brightness within a 3-arcsecond radius. This sample was then subject to two practical constraints. We needed all of our targets to have high-resolution HST imaging, which limited our choice to candidates in the innermost regions of the cluster. The 11-arcsecond proximity constraint ruled out some targets in the most crowded regions, forcing us to re-select from a reserve list. This left us with 29 galaxies inside the HST field of view and one outside (galaxy 20). Each plate was exposed five times for two hours, for a total of ten hours per galaxy. The observations were carried out in visitor mode, which proved to be both efficient and accurate in terms of object acquisition. Excellent seeing of 0.60 arcseconds reduced the correlation between neighbouring spaxels.

Our sample is biased towards bright objects, which in turn could bias us to detect more SRs. We simulated observations of the Virgo Cluster (for which the SR population is known from ATLAS^{3D}) using the luminosity function of our sample. This showed that we could recover the true value of f_{SR} for Abell 1689. Although we did not do a colour selection, our sample falls entirely on the Red Sequence (RS). However, the number of galaxies that do not fall on the RS in Abell 1689 is extremely low, and we found the bias to be minimal.

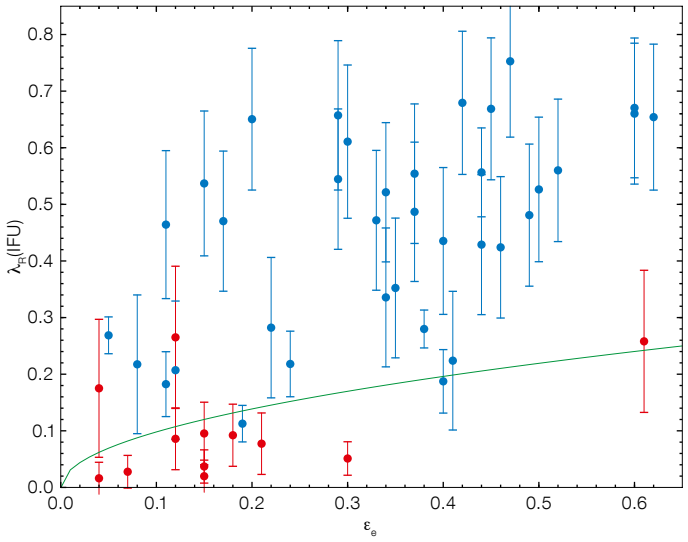

Figure 2. λ_R(IFU) *vs.* ε_e for the simulated observations of the SAURON sample of galaxies. The green lines separate SRs (below) from FRs. Red and blue circles denote SRs and FRs respectively, according to the original SAURON classification (Emsellem et al., 2007). Due to the different observing setup, some galaxies have been misclassified: these are the red dots above the green line and the blue dots below.

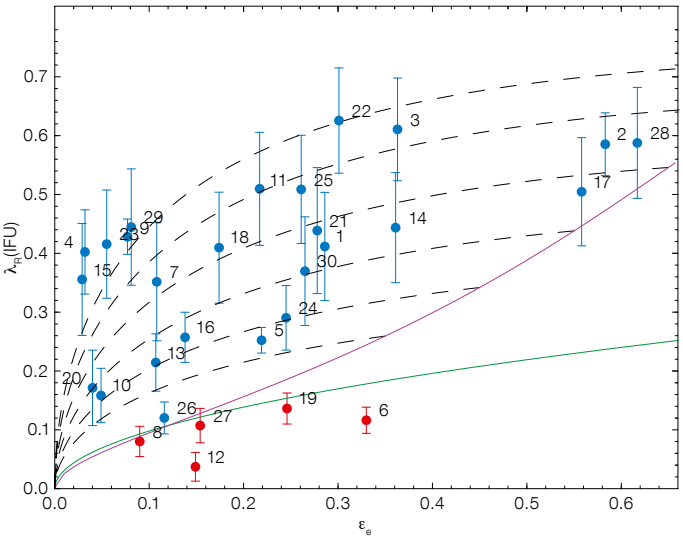

Figure 3. λ_R(IFU) *vs.* ε_e for all target galaxies in Abell 1689. The green line separates FRs (blue dots above) from SRs (red dots below). The magenta and dashed lines represent the view of an axisymmetric galaxy, edge-on and at various inclinations. Details about these models are given in Cappellari et al. (2007) and Emsellem et al. (2011).

To reduce the FLAMES/GIRAFFE data we used the official ESO pipeline[1], following the guidelines ESO offers[2]. Stellar kinematics were extracted using pPXF[3]; we used a line-of-sight velocity dispersion (LOSVD) expressed by a Gaussian function, obtaining just the velocity V and velocity dispersion σ. The stellar template library of choice was the high-resolution version (R = 40 000) of the ELODIE template library[4].

Slow and fast rotators at z = 0.18

Figure 1 shows the resulting kinematic maps. Although the spatial resolution is low (compared to SAURON) rotation can be clearly seen in some galaxies, and not in others.

Since our spatial resolution is coarse, we cannot detect kinematically decoupled cores (KDCs) and double σ peaks (2σ) as in Krajnovíc et al. (2011). If we try to detect SRs from the velocity maps by eye (as done by the SAURON and ATLAS^{3D} teams) we identify at most six: galaxies 4, 8, 12, 20, 26 and 27 (see Figure 1). The overall value of f_{SR} in the sample would then be 0.20, in line with what was found in the Virgo core (Cappellari et al., 2011b). However, contamination from face-on discs, which may appear as SRs, can bias the estimate.

Five more objects, despite exhibiting large-scale rotation, have misaligned kinematic and photometric axes, a feature more common in SRs than in FRs (Krajnovíc et al., 2011): these are galaxies 1, 3, 5, 9, 17 and 25 (Figure 1). Galaxies 3 and 17 have very high ellipticities, and are thus unlikely to be SRs, which have ellipticity $\varepsilon < 0.4$. Galaxy 5 has high velocity dispersion, and also contains an inner disc (R = 1.5 kpc) in the HST imaging.

λ_R measurements and kinematic classification

Emsellem et al. (2007) introduced the estimator λ_R to measure the projected specific angular momentum of galaxies; and Emsellem et al. (2011) further show how the combination of λ_R and ε conveniently captures the kinematic boundary between SRs and FRs. They define $\lambda_R(R_e)$ as the value of λ_R computed inside R_e, and use it in their $\lambda_R(R_e)$ *vs.* ε diagram.

In our study the galaxies are not sampled evenly, because R_e varies while the size of the IFUs is fixed. We cannot follow the ATLAS^{3D} prescription precisely and therefore introduced λ_R(IFU); defined as the value of λ_R computed using all the available spaxels in the IFU field of view. This introduces additional differences between our setup and that of ATLAS^{3D}, but we used existing SAURON data to determine how our observations and definition compare to those of ATLAS^{3D}. We made models of the SAURON galaxies using kinemetry[5] and, after projecting at redshift z = 0.183 and convolving with the seeing, we sampled them using the FLAMES/GIRAFFE setup. The resulting simulated data, after adding noise, have been used to measure λ_R, which we then compared with the original SAURON values to estimate both bias and systematic error.

We corrected λ_R(IFU) according to the bias measured and included the systematic error in quadrature with the random error. This correction takes into account both the different apertures between λ_R(IFU) and $\lambda_R(R_e)$ and the different spatial resolutions between λ_R(IFU) and ε_e. In Figure 2 we plot simulated values of λ_R(IFU) against published values of ε_e (Emsellem et al., 2007). Despite the aforementioned differences, there is little (< 10%) misclassification in our diagram, especially at high values of R_e. Given the known uncertainties, we can calculate the probability distribution for the

measured number of SRs in the SAURON survey (galaxies below the green line in Figure 2 defined by $0.31\sqrt{\varepsilon}$ and the green line in Figure 2, Emsellem et al. [2011]). We adopt a Monte Carlo approach (for each galaxy we assumed Gaussian errors in λ_R). The resulting probability distribution is Gaussian-like and we find 12.3 ± 1.7 slow rotators, where the true value is 12.

When we correct the values for our Abell 1689 data in the same way (Figure 3), we can similarly calculate the probability distribution for the number of SRs in Abell 1689. This analysis finds 4.5 ± 1.0 slow rotators, corresponding to f_{SR} = 0.15 ± 0.03.

Emsellem et al. (2007) warn about using only λ_R to assign a galaxy to either the slow or fast rotator class. The discrepancy between the classification "by eye" and the classification we adopted here underscores that warning. However, when studying galaxies beyond the local Universe, a detailed analysis such as that carried out by the ATLAS^{3D} team is not feasible. We are thus forced to rely on a statistical approach.

Slow rotators and environment density

For each galaxy in the sample we estimate the local environment density following Cappellari et al. (2011b). We define Σ_3 as the number density of galaxies inside the minimum circular area, centred on the target galaxy, and encompassing three other galaxies (down to a magnitude limit). Interlopers were dealt with by subtracting everywhere a constant mean value of Σ_3 = 0.49 galaxies per square arcminute. In Figure 4 we show f_{SR} versus $\log_{10}\Sigma_3$ for Abell 1689 (red), compared to the results of the ATLAS^{3D} survey (green; Cappellari et al., 2011b). The densest environment in ATLAS^{3D} (i.e., the core of the Virgo Cluster) has f_{SR} = 0.25, double that typically found in less dense environments ($f_{SR} \approx 0.12$).

In this study we probed environments with values of $\log_{10}\Sigma_3$ between 2.06 and 3.75: the minimum is comparable to the core of Virgo, and the maximum is 1.7 dex higher. In this respect our work

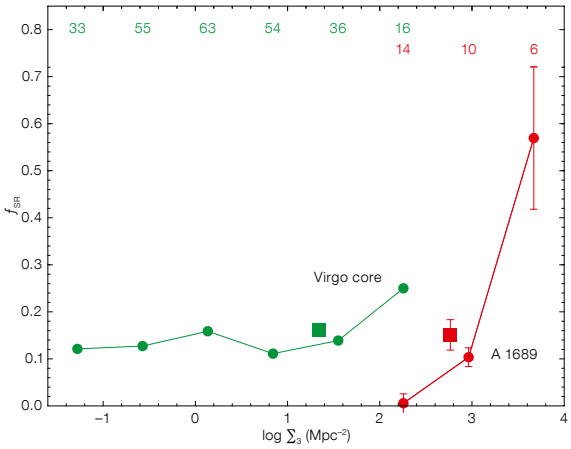

Figure 4. Fraction of slow rotators f_{SR} over the ETG population, as a function of the environment density. The green circles and line are from the ATLAS^{3D} survey (Cappellari et al., 2011b), red symbols are for Abell 1689. The numbers at the top give the total number of galaxies in each bin. The uncertainty in the SR classification is reflected in the error bars. The green square is the value of f_{SR} that we measure, resampling Virgo using our sample luminosity function. The error bars are smaller than the point size. The average fraction for Abell 1689 is shown by the red square.

starts exactly where ATLAS^{3D} finished. Abell 1689 shows a sharp increase in f_{SR} with projected density, from f_{SR} = 0.01 in the least dense environment to f_{SR} = 0.58 in the innermost regions. The densest bin in Abell 1689 has a higher fraction of SRs than the core of Virgo (Figure 4). The intermediate bin has a value of f_{SR} compatible with both the field/group environments and the overall Virgo cluster value, but is less than the Virgo core. f_{SR} in the least dense bin is lower than the ATLAS^{3D} field and group values.

Considering the whole Abell 1689 sample, we find an average value of $\log_{10}\Sigma_3$ = 2.77 and a SR fraction of 0.15 ± 0.03 (red square in Figure 4), which is the same as the overall SR fraction in the Virgo cluster, when sampled in the same way (green square). Furthermore, both values are similar to the field and group samples in ATLAS^{3D}, suggesting little to no difference in f_{SR} when it is averaged over an entire cluster population.

Abell 1689 has a higher average density than Virgo, but the same average slow rotator fraction f_{SR}. Inside the cluster, f_{SR} rises with projected density. In the least dense region, f_{SR} is significantly smaller than the ATLAS^{3D} field/group value. Given the low number of galaxies per bin, we cannot rigorously claim that this is representative. However, a similar "depletion" is observed in the outskirts of the Virgo cluster (Cappellari et al., 2011b). SRs are uniformly distributed across a range of environments; we know that they are on average more massive than FRs, and that dynamical friction is more efficient in objects with mass higher than the average particle mass. Hence the higher f_{SR} in the core of clusters is consistent with the effects of dynamical friction.

On account of the importance of the SR/FR division in understanding galaxy formation/evolution, it is crucial to expand this study, in particular by increasing the number of observed clusters, to quantify the scatter in f_{SR} and the radial variation within different clusters. Sampling clusters with different densities and dynamical states would give us great insight on the topic. Observations of the Abell 1650 cluster, with an intermediate mass, lying between that of Virgo and Abell 1689, are already scheduled at the VLT. Interesting times are ahead!

References

Bower, G., Lucey, J. R. & Ellis, R. S. 1992, MNRAS, 254, 613
Cappellari, M. et al. 2007, MNRAS, 379, 418
Cappellari, M. et al. 2011a, MNRAS, 413, 813
Cappellari, M. et al. 2011b, MNRAS, 416, 1680
Dressler, A. 1980, ApJ, 236, 351
Emsellem, E. et al. 2007, MNRAS, 379, 401
Emsellem, E. et al. 2011, MNRAS, 414, 818
Houghton, R. C. W. et al. 2012, MNRAS, 423, 256
Krajnovíc, D. et al. 2011, MNRAS, 414, 2923
Pasquini, L. et al. 2002, The Messenger, 110, 1

Links

[1] ESO Giraffe Pipeline: http://www.eso.org/sci/software/pipelines/giraffe/giraf-pipe-recipes.html
[2] Guidelines for Giraffe Pipeline: ftp://ftp.eso.org/pub/dfs/pipelines/giraffe/giraf-manual-2.8.7.pdf
[3] pPXF: http://www-astro.physics.ox.ac.uk/~mxc/idl/
[4] Elodie template library: www.obs-u-bordeaux1.fr/m2a/soubiran/elodie_library.html
[5] Kinemetry: www.davor.krajnovic.org/idl